Force and Stiffness Calculations in Magnetic Bearings – Comparison between Finite Element Method and Network Theory

E. Schmidt

Institute for Electrical Machines and Drives
University of Technology Vienna
Gusshausstrasse 25–29
Vienna A–1040, Austria

T. Platter, H. Springer

Institute for Machine Dynamics and Measurement
University of Technology Vienna
Wiedner Hauptstrasse 8–10
Vienna A–1040, Austria

Abstract

The paper presents two general modelling techniques for radial magnetic bearings which allow to consider the non-centered rotor position and the unsymmetric flux pattern. Both a finite element model and an enhanced network model are used to evaluate important bearing parameters for different rotor positions and control currents. The calculation results will be shown for a typical design of commercially available radial magnetic bearing actuators with four polepairs.

1 Introduction

Using the traditional model to obtain the force-displacement and force-current relationship for a magnetic bearing actuator, the flux densities in different polepairs of a magnetic bearing are calculated from independent magnetic circuits [1],[8]. In this modelling strategy the bearing consists of a number of horseshoe magnets without magnetic flux paths coupling the polepairs. In the symmetric bearing configuration with four polepairs the two resulting force equations in two orthogonal directions are uncoupled.

This paper describes two general modelling techniques which allow the non-centered rotor position and the unsymmetric flux pattern to be taken into consideration:

- *Electromagnetic finite element analysis* using independent coil current excitation and the multipoint constraint method to model the non-centered rotor at different angular positions.
- *Enhanced magnetic circuit model* with finite permeable magnetic flux paths in the stator and rotor backiron parts between adjacent polepairs.

The calculations are concerning the design (geometry, materials, coils) of commercially available radial magnetic bearing actuators with four polepairs. Both analyses are based on the following assumptions:

- The control currents in the coil pairs are constant in time and all calculations are performed at standstill. Because of the laminated rotor iron and a non-magnetic rotor-yoke smaller than the skin depth at maximum rotational speed, eddy current effects due to the shaft rotation cause no substantial changes in the magnetic flux distribution.
- The permeability of different iron parts is considered to be constant. Saturation of the magnetic circuit is not modelled, because common active magnetic bearings are not designed to run under this condition.
- The flux distribution in the axial direction of the bearing is supposed to be constant, fringing effects in the axial direction are not considered. Therefore, the calculation of the flux densities can be carried out by using two dimensional models.

Both, the non-centered rotor position and different control currents in the driving coils result in an unsymmetric flux pattern, even though the actuator is symmetric with respect to two orthogonal directions. Therefore, *coupling terms in the force-displacement and force-current relationship* between two orthogonal directions may appear. Using first order expansion, the actuator force equations in terms of coil current $\mathbf{i}$ and displacement $\mathbf{x}$ can be written in the general form

$$\mathbf{F}(\mathbf{i},\mathbf{x}) = \mathbf{F}(i_{Bias},\mathbf{i}_0,\mathbf{x}_0) + \mathbf{K}_i \cdot \mathbf{i} + \mathbf{K} \cdot \mathbf{x} \ , \qquad (1)$$

where current gain $\mathbf{K}_i$ and open loop stiffness $\mathbf{K}$ are written in more detail as

$$\mathbf{K}_i = \begin{bmatrix} K_{i,xx} & K_{i,xy} \\ K_{i,yx} & K_{i,yy} \end{bmatrix} \ , \quad \mathbf{K} = \begin{bmatrix} K_{xx} & K_{xy} \\ K_{yx} & K_{yy} \end{bmatrix} \ . \qquad (2)$$

The calculated results for the bearing parameters magnetic force $\mathbf{F}$ and current gain $\mathbf{K}_i$ are compared between the two dimensional finite element model and the network model for different rotor positions $\mathbf{x}_0$.

2 Modelling methods

2.1 Electromagnetic finite element analysis

In the two dimensional finite element model Fig. 1 the non-centered rotor position has to be considered. This is carried out by using different cylindrical coordinate systems for stator and rotor geometry and a sophisticated

modelling of the air gap. The air gap is cut into two parts along a circular line concentric to the stator. The outer part is meshed with the stator, the inner part with the rotor. Both, the stator and the rotor model have equidistant nodes in the angular direction on the common circular boundary. The two models are connected using a set of multipoint constraints for the unknown magnetic vector potential at the corresponding nodes. For each radial rotor position of interest only one finite element model is generated. Due to the equidistant nodes on the common boundary, an *arbitrary angular rotor position* can be calculated by shifting the multipoint constraint connections [4].

For the whole model eight node quadrilateral and six node triangular isoparametric elements are employed. The magnetic materials (pole legs, stator backiron, rotor and shaft) are treated to be linear with constant permeabilities. The excitation is modelled by applying independent source current densities equivalent to the product of coil current and the number of turns for each stator coil. So, there is no restriction on the combination of the coil current distribution.

The governing equations for the magnetic vector potential are solved using the linear magnetostatic analysis from the finite element software MSC/EMAS [7].

The *magnetic force* $\mathbf{F}$ acting on the rotor surface is obtained from the field solution within the air gap by integrating the Maxwell stresses over the rotor surface [6]. In terms of cylindrical coordinates (unit vectors $\vec{e}_r$,$\vec{e}_\varphi$), the local Maxwell stresses on the rotor surface are given by

$$\mathbf{p}(\varphi) = \frac{1}{2\mu_0}\left((B_r^2 - B_\varphi^2)\,\vec{e}_r + 2B_r B_\varphi\,\vec{e}_\varphi\right) \quad . \tag{3}$$

Both, the normal component and the tangential component of the flux density within the air gap are taken into account.

2.2 Enhanced magnetic circuit model

Neglecting leakage and fringing effects, the magnetic flux paths of the magnetic bearing are well defined. Assuming constant flux density over the cross section in the different flux paths of the bearing (airgap, pole legs, stator backiron, rotor and rotor-yoke), the radial magnetic bearing actuator can be modelled as a network of magnetic reluctances [3],[5]. In addition to the commonly used independent equivalent magnetic circuit for each polepair, magnetic reluctances for the flux paths in the stator and rotor backiron parts between adjacent polepairs are considered. Therefore, the magnetic flux paths are represented within *one equivalent magnetic circuit for the whole magnetic bearing* as depicted in Fig. 2.

In the derived magnetic circuit the iron paths are *finite permeable* with constant permeability. Different permeabilities for the stator and rotor iron can be introduced if necessary. The circuit is excited with the product Θ of coil current and the number of turns for each stator coil. By applying the law of conservation of magnetic flux and Ampere's loop law, a system of algebraic equations can be found to evaluate the unknown magnetic flux distribution. The resulting system of algebraic equations

$$\mathbf{R}\cdot\mathbf{\Phi} = \mathbf{\Theta} \tag{4}$$

is linear due to the constant permeabilities in the iron paths.

The *magnetic force* $\mathbf{F}$ exerted on the rotor surface is the vector sum of the forces within the eight air gaps. The local Maxwell stresses on the rotor surface now becomes

$$\mathbf{p}(\varphi) = \frac{B_r^2}{2\mu_0}\,\vec{e}_r \quad , \tag{5}$$

because from the magnetic circuit theory, the flux densities have only a normal component on the rotor surface. The flux densities are obtained directly from the flux distribution in the air gap.

2.3 Force and stiffness calculation

Due to the linearity of the problem, it is not meaningful to calculate the force for any possible coil current combination at each interesting rotor position $\mathbf{x}_0$. Instead, the relationship between the force and the four individual coil currents can be described as a quadratic form for each force component,

$$\mathbf{F} = \begin{bmatrix} F_x \\ F_y \end{bmatrix} = \begin{bmatrix} \mathbf{i}_{Coil}^T \cdot \mathbf{X}_x \cdot \mathbf{i}_{Coil} \\ \mathbf{i}_{Coil}^T \cdot \mathbf{X}_y \cdot \mathbf{i}_{Coil} \end{bmatrix} \quad , \tag{6}$$

with both presented modelling methods for each rotor position considered.

The two 4×4 symmetric force matrices $\mathbf{X}_x$,$\mathbf{X}_y$ for the finite element model are obtained in one solution sequence by using capabilities of the MSC/EMAS software. The evaluation of the two 4×4 symmetric force matrices for the magnetic circuit model is completely carried out from the algebraic system of linear equations Eq. (4) with matrix calculus by using the MATLAB package.

Usually, instead of four independent coil currents

$$\mathbf{i}_{Coil} = \begin{Bmatrix} i_{Coil,1} \\ i_{Coil,2} \\ i_{Coil,3} \\ i_{Coil,4} \end{Bmatrix} \tag{7}$$

two control currents in the orthogonal directions and the bias current as

$$\mathbf{i}_C = \begin{Bmatrix} i_x \\ i_y \\ i_{Bias} \end{Bmatrix} \tag{8}$$

are used to desribe the current injection. The transformation is defined as

$$\mathbf{i}_{Coil} = \begin{bmatrix} +1 & 0 & 1 \\ 0 & +1 & 1 \\ -1 & 0 & 1 \\ 0 & -1 & 1 \end{bmatrix} \cdot \mathbf{i}_C \quad . \tag{9}$$

Therefore, the force components Eq. (6) can be written as quadratic forms with regard to control and bias currents $\mathbf{i}_C$ too. With the introduction of new symmetric 3×3 matrices $\mathbf{X}_x^C$,$\mathbf{X}_y^C$ the force components at the considered rotor position $\mathbf{x}_0$ are calculated from

$$\mathbf{F}(\mathbf{i}_C, \mathbf{x}_0) = \begin{bmatrix} F_x \\ F_y \end{bmatrix} = \begin{bmatrix} \mathbf{i}_C^T \cdot \mathbf{X}_x^C \cdot \mathbf{i}_C \\ \mathbf{i}_C^T \cdot \mathbf{X}_y^C \cdot \mathbf{i}_C \end{bmatrix} \quad . \tag{10}$$

Furthermore, the *current gain* $\mathbf{K}_i$ can be calculated directly from the symmetric force matrices $\mathbf{X}_x^C$,$\mathbf{X}_y^C$ for any applied control and bias currents. Due to the symmetic matrices, the first order expansion Eq. (1) yields the current gain in terms of control and bias currents $\mathbf{i}_C$ in the form

$$\mathbf{K}_i(\mathbf{i}_C, \mathbf{x}_0) = \begin{bmatrix} \mathbf{i}_C^T \cdot \mathbf{X}_x^C \\ \mathbf{i}_C^T \cdot \mathbf{X}_y^C \end{bmatrix} \cdot \begin{bmatrix} 2 & 0 \\ 0 & 2 \\ 0 & 0 \end{bmatrix} \qquad (11)$$

for both modelling methods presented.

A particular refinement of the magnetic circuit model is, that *open loop stiffness* $\mathbf{K}$ can be calculated analytically as a differential quotient at the actual control and bias currents $\mathbf{i}_C$ and the actual rotor position $\mathbf{x}_0$. No difference quotient has to be calculated and therefore numerical problems can be avoided.

3 Numerical results

The chracteristic bearing parameters magnetic force $\mathbf{F}$ and current gain $\mathbb{K}_i$ are evaluated considering the design of a commercially available radial magnetic bearing actuator with four polepairs as depicted in Fig. 1. The enhanced magnetic circuit model with finite permeable magnetic flux paths in the stator and rotor backiron parts between adjacent polepairs is shown in Fig. 2.

Throughout the presented calculation results a non-centered rotor position with an *eccentricity* $\epsilon = 0.2\,\mathrm{mm}$ at *different angular positions* ϕ is assumed. The numerical results are shown only for one quadrant of angular position values. Due to the symmetric geometry and current injection in the two orthogonal directions x,y, the results for other rotor positions can be obtained by a meaningful interpretation of the evaluated values corresponding to the directions x,y. Also, the force-current relationships and the current gains for $\pi/2 \leq \phi \leq 2\pi$ may be easily deduced from a cyclic permutation of the results for $0 \leq \phi \leq \pi/2$.

3.1 Force calculation

Fig. 3 shows the magnetic force component F_x in the horizontal direction obtained from the finite element model for different values of the rotor position angle ϕ. Thereby, the control current i_x in the horizontal direction is varied while the control current i_y in the vertical direction and the bias current i_{Bias} are kept constant. The angular rotor position significantly influences the absolute force value. Only for the 90° position a linear force-current relationship is obtained. All other rotor positions result in quadratic control current characteristics.

These relationships are obtained also from the magnetic circuit model. A comparison between the two modelling methods regarding the horizontal force component F_x is shown in Fig. 4. There is a good agreement in the force component F_x between the two models.

Fig. 5 shows the magnetic force component F_y in the vertical direction obtained from the finite element model for different values of the rotor position angle ϕ. Thereby, the control current i_x in the horizontal direction is varied while the control current i_y in the vertical direction and the bias current i_{Bias} are kept constant. The absolute force value increases with increasing position angle ϕ because of the decreasing airgap lengths in the lower vertical polepair. The effect of the variing control current i_x is small compared with the influence of the bias current i_{Bias}.

Similar relationships are obtained from the magnetic circuit model. A comparison between the two modelling methods for the vertical force component F_y is shown in Fig. 6. As the network method does not account for circumferential magnetic flux densities within the airgaps, the slight difference between the two methods would be expected from Eq. (3) and Eq. (5).

3.2 Actuator gain calculation

Fig. 7 shows the actuator gains in terms of the bias current i_{Bias} with no control currents i_x,i_y as obtained from the finite element model. As known from the analysis for a centered rotor position, there is a linear relationship between actuator gain and bias current. This is true for the non-centered rotor position too. However, the angular rotor position ϕ has a strong influence on the gain magnitude. Because of the non-centered rotor position, cross-coupling terms in the current gain $\mathbf{K}_i$ appear. However, they are negligible small compared with the main diagonal terms. The main diagonal terms are evaluated by both methods with good agreement as shown in Fig. 8. As mentioned above, the network method does not account for circumferential magnetic flux densities within the airgaps. Therefore, the cross-coupling terms are not calculated correctly by the magnetic circuit model as shown in Fig. 8.

The calculated characteristics of the current gain $K_{i,xx}$ in terms of the control current i_x (as obtained from the finite element model) in Fig. 9 are closely related to the relationships of the force component F_x in Fig. 3. Only for the 90° position of the rotor a constant value is obtained. All other rotor positions result in linear control current characteristics. This is caused by the non-centered rotor position. The agreement between the two modelling methods (Fig. 10) is nearly as good as for the force component F_x, see Fig. 4.

The gain cross-coupling terms $K_{i,xy}$ as a function of the control current i_x as obtained from the finite element model are shown in Fig. 11. As expected, the control current affects the actuator gain much stronger than the bias current (compare Fig. 7). The comparsion between the cross-coupling gains calculated from both methods is shown in Fig. 12. Nearby the zero crossing of a cross-coupling term value, the calculated ratios are not meaningful because of numerical rounding errors. However, aside the zero crossing vicinity noticeable differences between the two modelling methods are again based on the different formulas Eq. (3),Eq. (5) for the maxwell stresses within the airgaps.

4 Conclusions

The two general modelling techniques presented allow to consider non-centered rotor positions and unsymmetric flux patterns in magnetic bearings. Important bearing parameters as magnetic force $\mathbf{F}$ and current gain $\mathbf{K}_i$ are

evaluated for various rotor positions and control currents. Thereby, the bias current can be considered as a parameter.

Numerical results obtained from both a two dimensional finite element model and a network model are compared. The aim of the comparison is to validate the magnetic circuit model that neglects leakage flux paths and fringing effects. The two methods presented agree closely in the magnetic force characteristics $\mathbf{F}$ and in the main diagonal terms of the actuator gain $\mathbf{K}_i$. There are noticeable differences, however, in the cross-coupling terms of the actuator gain $\mathbf{K}_i$.

Since the theory of radial magnetic bearings with centered rotor postion considers only the main diagonal terms of the actuator gain, the magnetic circuit model is applicable with less effort compared with the finite element model.

Only with the full utilization of linearity the finite element solutions can be treated as an economic tool to calculate magnetic force and actuator gain. Using a sophisticated modelling of the air gap, only one finite element model is generated for each radial rotor position of interest. The different angular positions of the non-centered rotor are modelled with the multipoint constraint method. The finite element model gains in significance when concerning non-centered rotor positions because of more accurate results for magnetic force and actuator gain.

References

[1] Allaire P.E., Maslen E.H., Humphris R.R., Knospe C.R., Lewis D.E.: "Magnetic Bearings". *CRC Handbook of Lubrication and Tribology*, Vol.3, 1994.

[2] Allaire P.E., Rockwell R., Kasarda M.E.F.: "Magnetic and Electric Field Equations for Magnetic Bearing Applications". *Proceedings of the 5th International Symposium on Magnetic Bearings*, Virginia, 1995.

[3] Gähler C., Förch P.: "A Precise Magnetic Bearing Exiter for Rotordynamic Experiments". *Proceedings of the 4th International Symposium on Magnetic Bearings*, ETH Zürich, 1994.

[4] Jin J.M.: *The Finite Element Method in Electromagnetics.* John Wiley, 1993.

[5] Maslen E.H., Meeker D.C.: "Fault Tolerance of Magnetic Bearings by General Bias Current Linearization". *IEEE Transactions on Magnetics*, Vol.31, May 1995.

[6] Moon F.C.: *Magneto-Solid Mechanics.* John Wiley & Sons, New York, 1984.

[7] *MSC/EMAS Users Manual, Version 3.* The MacNeal-Schwendler Corporation, Los Angeles, 1994.

[8] Schweitzer G., Traxler A., Bleuler H.: *Magnetlager, Grundlagen, Eigenschaften und Anwendungen berührungsfreier, elektromagnetischer Lager.* Springer Verlag, Berlin, 1993.

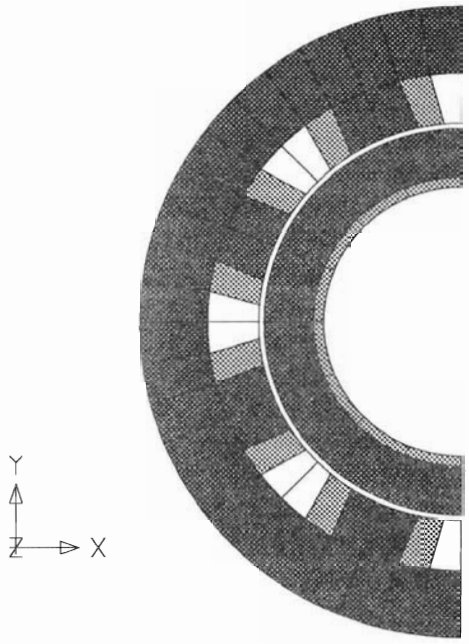

Fig. 1: Geometry (left half) of the finite element model

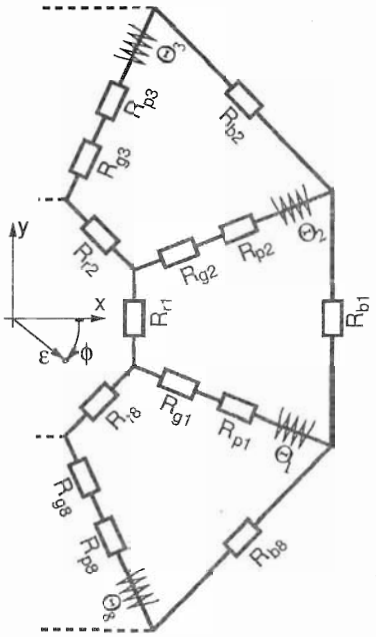

Fig. 2: Enhanced magnetic circuit model (right half)

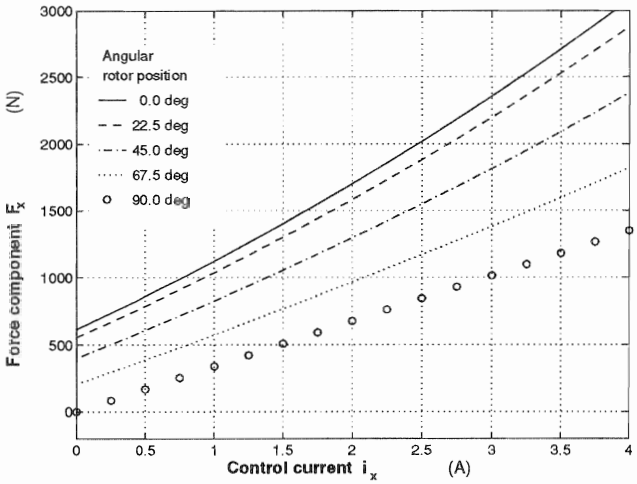

Fig. 3: Horizontal force F_x (FEM), $\epsilon = 0.2\,\mathrm{mm}$, bias current $i_{Bias} = 4\,\mathrm{A}$, control current $i_y = 0\,\mathrm{A}$

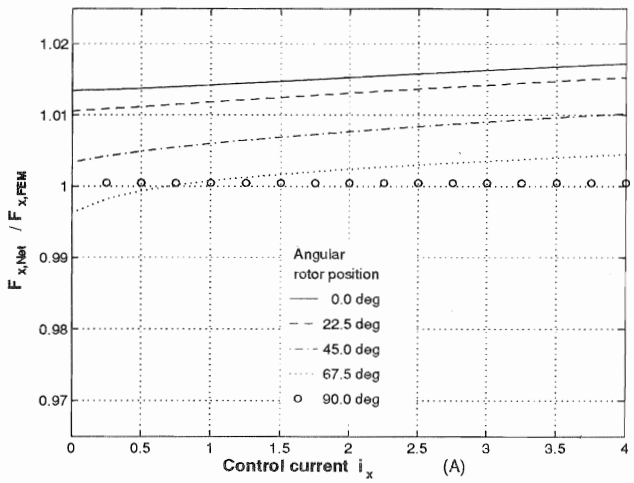

Fig. 4: Network-FEM ratio F_x, $\epsilon = 0.2\,\mathrm{mm}$, bias current $i_{Bias} = 4\,\mathrm{A}$, control current $i_y = 0\,\mathrm{A}$

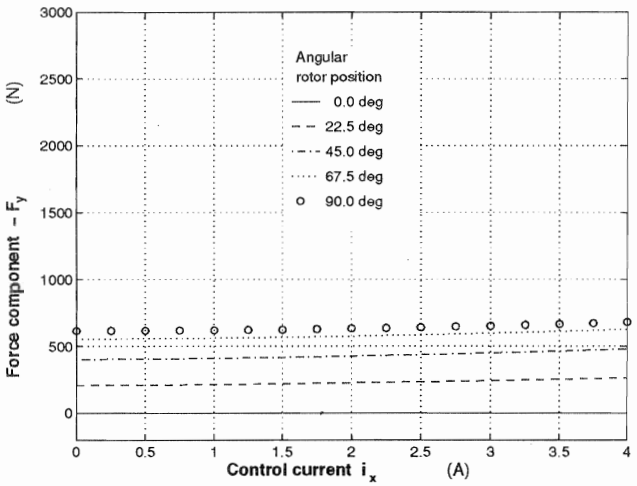

Fig. 5: Vertical force F_y (FEM), $\epsilon = 0.2\,\mathrm{mm}$, bias current $i_{Bias} = 4\,\mathrm{A}$, control current $i_y = 0\,\mathrm{A}$

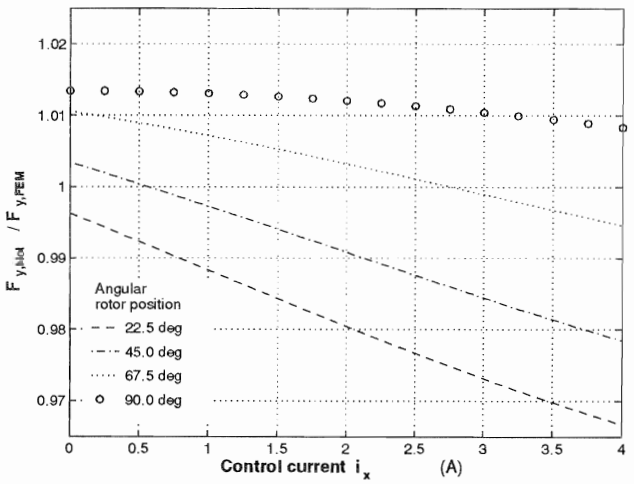

Fig. 6: Network-FEM ratio F_y, $\epsilon = 0.2\,\mathrm{mm}$, bias current $i_{Bias} = 4\,\mathrm{A}$, control current $i_y = 0\,\mathrm{A}$

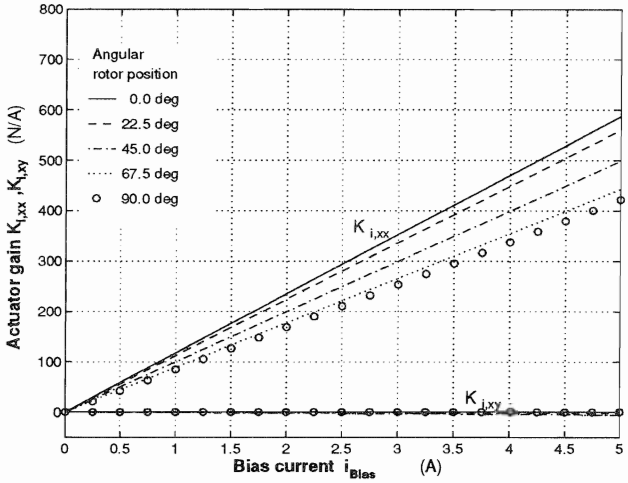

Fig. 7: Actuator gain $K_{i,xx}$ (FEM), $\epsilon = 0.2\,\mathrm{mm}$, no control currents

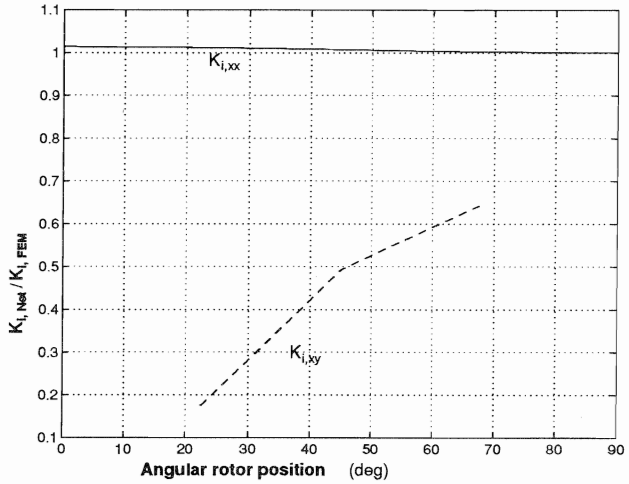

Fig. 8: Network-FEM ratio, $\epsilon = 0.2\,\mathrm{mm}$, no control currents, no bias current dependency

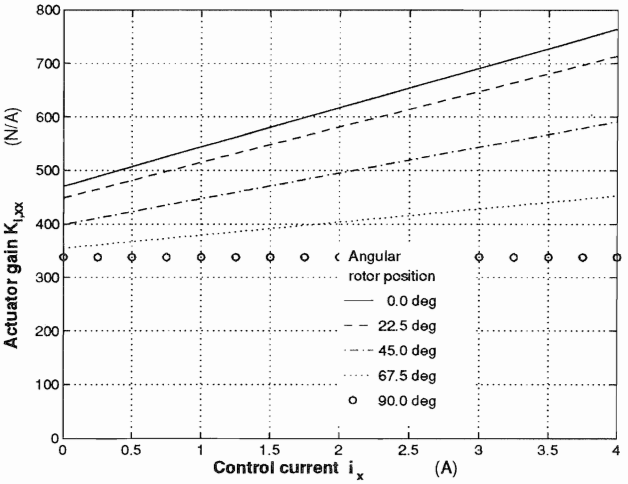

Fig. 9: Actuator gain $K_{i,xx}$ (FEM), $\epsilon = 0.2\,\mathrm{mm}$, bias current $i_{Bias} = 4\,\mathrm{A}$, control current $i_y = 0\,\mathrm{A}$

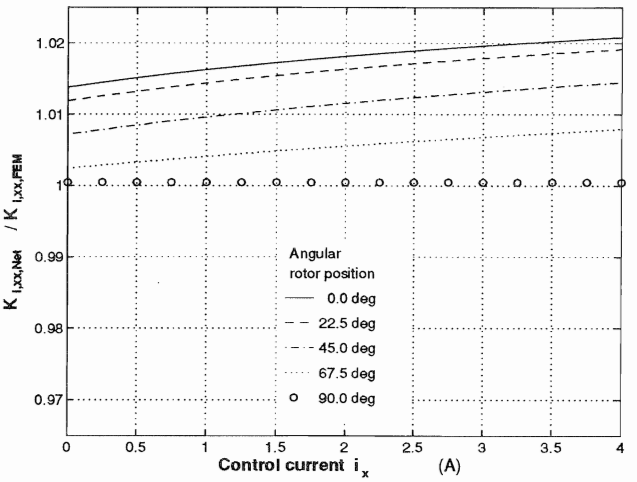

Fig. 10: Network-FEM ratio $K_{i,xx}$, $\epsilon = 0.2\,\mathrm{mm}$, bias current $i_{Bias} = 4\,\mathrm{A}$, control current $i_y = 0\,\mathrm{A}$

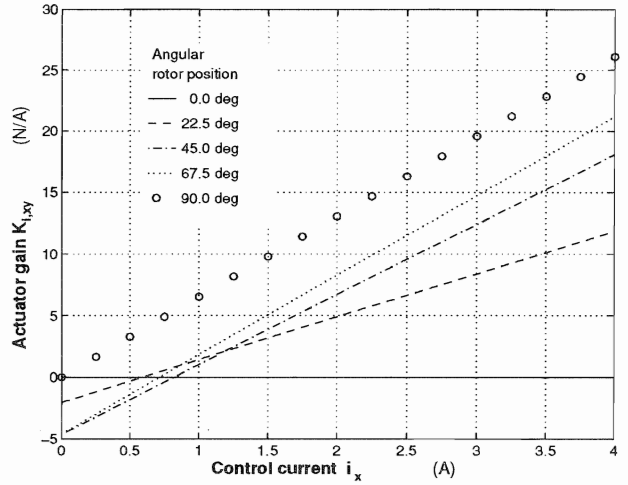

Fig. 11: Actuator gain $K_{i,xy}$ (FEM), $\epsilon = 0.2\,\mathrm{mm}$, bias current $i_{Bias} = 4\,\mathrm{A}$, control current $i_y = 0\,\mathrm{A}$

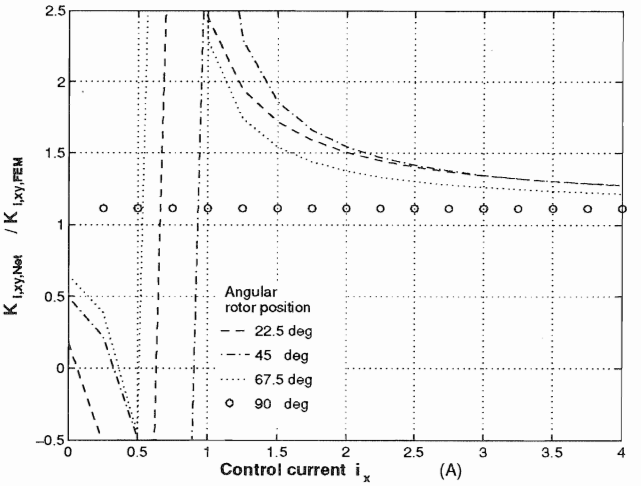

Fig. 12: Network-FEM ratio $K_{i,xy}$, $\epsilon = 0.2\,\mathrm{mm}$, bias current $i_{Bias} = 4\,\mathrm{A}$, control current $i_y = 0\,\mathrm{A}$